ACS OMEGA

http://pubs.acs.org/journal/acsodf

Article

Pyrolysis Behavior of Pyrite under a CO−H_2 Atmosphere

Zhuang Zheng, Yang You,* Jiabao Guo, Gang Li, Zhixiong You, and Xuewei Lv*

Cite This: *ACS Omega* 2022, 7, 29116−29124

Read Online

ACCESS | Metrics & More | Article Recommendations

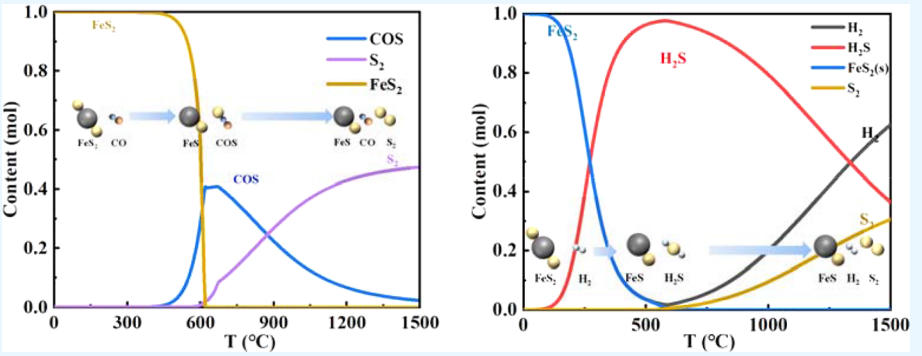

ABSTRACT: The transformation behavior of pyrite (FeS_2) in the blast furnace process is critical to control the formation and emission of gaseous sulfides in the top gas of ironmaking but has seldom been explored. In present work, the pyrolysis of pyrite from 200 to 900 °C under a CO−H_2 atmosphere was investigated by thermal-gravimetric and mass spectrometry. The thermodynamic theoretical calculations were carried out to further understand the transformation process. The results show that FeS_2 is almost completely reduced to FeS under various CO−H_2 atmospheres. H_2S and carbonyl sulfide (COS) are the main gaseous sulfides formed through the pyrolysis reactions of FeS_2 under a CO−H_2 atmosphere. A higher H_2 concentration can reduce the pyrolysis reaction temperature of FeS_2, which is favorable for the conversion of sulfides to H_2S, while a higher CO concentration promotes the conversion of sulfides to COS. Besides, the pyrolysis products of FeS_2 by order from the former to latter under a strong reductive atmosphere (CO−H_2) with increasing temperature are as follows: COS → S → H_2S → S_2 → CS_2.

1. INTRODUCTION

Gaseous sulfur emitted from industrial production processes from industries such as chemical, metallurgical, and power industries is one of the culprits that endanger the natural environment and human health.[1−3] Hence, environmental protection regulations for gaseous sulfide emissions from industrial production processes are becoming increasingly stringent all over the world. Blast furnace gas (BFG), as a combustible by-product of the ironmaking process, is an important secondary energy. Its main components are 20−28% CO, 17−25% CO_2, 50−55% N_2, 1−5% H_2,[4] 86−118 mg/Nm^3 hydrogen sulfide (H_2S), and 20−60 mg/Nm^3 carbonyl sulfide (COS).[5,6] Sulfides in BFG cause the corrosion of gas pipes and generator rotor blades.[7−9] Generally, it is better to remove the sulfides from the BFG before combustion.

Sulfur in the blast furnace comes from the burdens such as coke (over 70%), coal, and iron ore,[10,11] and its final destination is mainly the blast furnace slag, hot metal, and BFG. Organic sulfur (thiophenes, sulfoxides, and sulfones) and inorganic sulfur (pyrite and sulfate sulfur) are two common forms of sulfur in the coke.[12] Most of the sulfides in the burdens eventually enter into the slag and the hot metal, and the remaining small amount enters the BFG.[11] Although less sulfides enter the gas phase, the desulfurization process of the gas is more complex and thus has received extensive attention. Especially in the lumpy zone (200−900 °C) of blast furnace, the pyrite in the coke and iron ore is pyrolyzed in a reducing atmosphere to generate H_2S and COS, which is one of the main sources of sulfides in BFG.[13] Hence, the key to BFG desulfurization is the removal of H_2S and COS. It was reported that the removal difficulty of COS is significantly higher than that of H_2S, and COS usually needs to be converted into H_2S before the removal.[7,9,14] Therefore, exploring the decomposition mechanism of pyrite in a reducing atmosphere and controlling more pyrite in coke and iron ores to be converted into H_2S in the lumpy zone can help to achieve high-efficiency desulfurization of BFG.

Received: May 13, 2022
Accepted: August 2, 2022
Published: August 8, 2022

The pyrolysis of pyrite under different atmospheric conditions has been extensively studied.[15−19] Lv et al.[20] proposed that the decomposition of FeS_2 in a CO_2 atmosphere can be divided into three stages: $3FeS_2 \rightarrow 2FeS_2 + Fe_{1-x}S \rightarrow FeS_2 + Fe_{1-x}S + Fe_{1-y}S \rightarrow Fe_{1-x}S + 2Fe_{1-y}S$. Moreover, CO_2 promotes the decomposition of FeS_2, and the product S further reacts with CO_2 to form COS. Huang et al.[16] found that FeS_2 began to decompose at 560 °C in a CO_2 atmosphere, and the type of solid products changes with the temperature. Particularly, pyrrhotite (FeS_x, $1 \leq x \leq 2$) is the only solid product when the temperature is lower than 700 °C, while the solid products change to magnetite (Fe_3O_4) and FeS for a temperature higher than 700 °C. Levy et al.[17] studied the reaction of pyrite with water vapor; pyrite reacted with water vapor to produce sulfur dioxide and H_2S at 440 °C, and the generated sulfur dioxide and H_2S further reacted to produce sulfur vapor and water. Hong et al.[21] investigated the decomposition of pyrite in He, N_2, CO_2−CO−SO_2, O_2−CO, and H_2S−H_2 gas mixtures from 400 to 590 °C. They concluded that pyrite decomposes to pyrrhotite and sulfur vapor in all atmospheres, and the decomposition can be divided into two processes: the formation of pyrrhotite and liquid sulfur and the gasification of liquid sulfur. Previous studies have basically confirmed that although pyrite can be decomposed in any atmosphere, the decomposition mechanism under different atmospheres varies significantly, and temperature is another important factor affecting the decomposition of pyrite. However, previous studies mainly focused on the pyrolysis of pyrite in inert and oxidizing atmospheres, and the studies on reducing atmospheres, especially H_2−CO mixed atmospheres, are still scarce.

In the present study, thermodynamic calculations and experiments were carried out to study the pyrolysis process of FeS_2 under the atmosphere of CO and H_2. The effects of temperature and H_2 ratio on the pyrolysis products including solid and gaseous products were analyzed to explore the transformation mechanism of sulfides in the blast furnace.

2. METHODS

2.1. Materials. Analytically pure pyrite with the size of 63−75 μm was used in the experiments. The purity of the pyrite was higher than 95 wt %, and the parameters of pyrite sample are shown in Table 1. X-ray diffraction (XRD) [model D/max2500/PC (Cu Kα)] analysis was performed to verify phase compositions of the sample. The detection was performed at an angular range of 20−90° with a scan rate of 4°/min, and the results are shown in Figure 1. In comparison of the standard phase, the pyrite samples used are with high purity. Besides, the impurities in the sample are mainly small amounts of silica and traces of calcium sulfide (shown in Figure 4). Due to the high stability of impurities under the current experimental conditions, the effect of impurities on the experimental results can be negligible.

Table 1. Parameters of Pyrite Samples

composition	standard value (wt %)	actual value (wt %)
FeS_2	≥95.0	96.5
Fe	≥43.0	44.2
S	≥52.0	52.3
Si	≤2.0	1.5
other		2

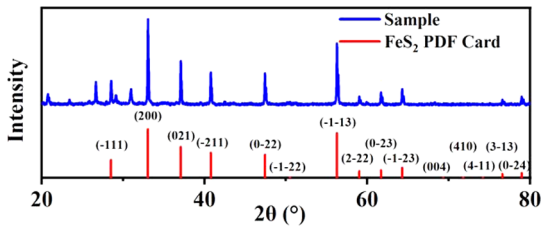

Figure 1. Comparison of the XRD pattern of the sample with the standard PDF card.

2.2. Experimental Procedures. The pyrolysis of pyrite was carried out in a thermo-gravimetric analyzer (Setaram Evo TG-DTA 1750) consisting of a vertical furnace, a gas manometer system for controlling the atmosphere in the reactor, and an electronic balance connected to a computer that records the mass loss. The schematic diagram of the thermo-gravimetric analyzer is similar to that of the previous study.[12,22−25] The reacted gas in the thermo-gravimetric analyzer was blown into a quadrupole mass spectrometer (TILON LC-D200, AMETEK LLC, USA) to detect its components according to the molecular weight. The electron ionization voltage, the temperature of the transfer line, and the m/z range of the mass spectrometer are 10−70 eV, 270 °C, and 1−200, respectively. Six different volume ratios (CO/H_2 = 100:0, 90:10, 75:25, 50:50, 25:75, and 10:90) of CO and H_2 mixtures were blown into the thermo-gravimetric analyzer as the reaction atmosphere. The protective gas was Ar (99.999%), and the gas flow rate was set at 20 mL/min to ensure that the gas could be carried away in time and avoid the impact of the secondary reaction on the instantaneous weight loss of the samples. For each test, the pyrite with an initial mass of 375 mg was placed into an alumina crucible (Φ 12 × 10 mm). The reaction vessel was evacuated to vacuum with a pump, and Ar (99.999%) was introduced into the reactor at a flow rate of 20 mL/min until the operating pressure reached 1 atm. The samples were heated from room temperature to 900 °C with 5 °C min^{-1} heating rate, and the mass loss was recorded until the end of the reduction. The final solid product after pyrolysis was detected by XRD to explore the change of sulfur in the solid samples after pyrolysis and the effect of reaction conditions on the precipitation of sulfur from pyrite.

2.3. Thermodynamic Calculation. In order to better understand the decomposition process of the pyrite, the final equilibrium state of pyrite in two mixed atmospheres (CO/H_2 = 25:75, 75:25) was calculated by FactSage software with the equilib module and the FactPS + FToxid databases. The ideal gas, pure liquids, and pure solids were selected as the reactants, and the temperature range was 0−1500 °C. Finally, thermodynamic calculation results can further explain the Experimental Results.

3. RESULTS AND DISCUSSION

3.1. Pyrolytic Behavior of FeS_2. To facilitate the analysis of the pyrolysis process of pyrite, its decomposition in a pure CO atmosphere is discussed as the base case. Figure 2 shows the thermo-gravimetry (TG) and derivative thermo-gravimetry (DTG) curves of pyrite in a pure CO atmosphere. It can be found that about 27% of the pyrite sample is decomposed into volatiles according to the mass loss curve. In addition, the mass loss rates (%/s) of FeS_2 are chosen to compare the reaction rates for different heating rates and plotted in Figure 2. Four

https://doi.org/10.1021/acsomega.2c02991
ACS Omega 2022, 7, 29116−29124

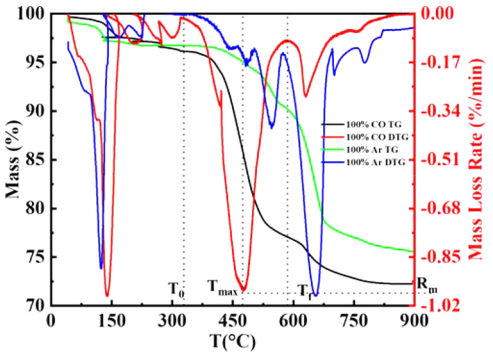

Figure 2. TG and DTG curves of pyrite pyrolysis in CO and Ar atmospheres.

parameters are used to describe the whole decomposition process, the starting temperature of the pyrolysis reaction (T_0), the final temperature of the pyrolysis reaction (T_f), the maximum mass loss rate (R_m), and the temperature corresponding to the maximum mass loss rate (T_{max}). Sahu et al.[26] defined the ignition temperature and the burn-up temperature as the temperature at which the mass loss rate of the combustion reaction first reaches 1%/min in the early and final stages, respectively. Similarly, the starting temperature and the final temperature of the pyrolysis reaction were obtained in the same way with a reference mass loss rate of 0.1%/min for FeS_2 in this work.

As shown in Figure 2, at the stage of 50−300 °C, the evaporation of water and the pyrolysis of a small amount of pyrite mainly occur. Most of the pyrolysis of pyrite occurs at 350−900 °C, so the discussions of this work focus on this stage. In addition, the pyrolysis of FeS_2 under an inert atmosphere (Ar) was carried out for comparison with CO. It can be found that the decomposition temperature of FeS_2 in CO is lower and the reaction is more thorough. This is because the S produced by the decomposition continues to react with CO so that the decomposition reaction moves in the direction of producing gas, thereby accelerating the process of decomposition.

It should be noted that TG and DTG curves show a reciprocating variation in the range of 150−300 °C. This is because the heating mode of the thermo-gravimetric analyzer is controlled by the proportional integral derivative (PID) system. In the PID mode, the process of increasing temperature with time is not linear but oscillating. During

Table 2. Characteristic Temperatures (T_0 and T_{max}) and R_m in Different Atmospheres

atmosphere	T_0 (°C)	T_{max} (°C)	R_m (%/min)
100% CO	331.75	475.47	−0.96
90% CO 10% H_2	330.04	480.83	−0.95
75% CO 25% H_2	334.06	490.40	−1.00
50% CO 50% H_2	333.54	501.01	1.03
25% CO 75% H_2	332.50	505.76	−1.15
10% CO 90% H_2	335.32	507.12	−1.19

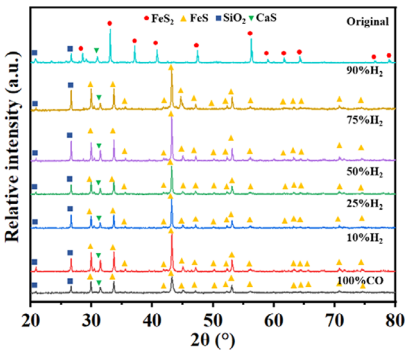

Figure 4. XRD patterns for the solid products formed at different gas compositions.

the heating process, the actual temperature may be higher or lower than the set temperature and gradually approaches the set temperature. Due to the hysteresis of heating control, the temperature fluctuation is more obvious in the range of 150−300 °C. Nevertheless, since the decomposition temperature of FeS_2 detected in the experiments is higher than 350 °C, the temperature fluctuation at this stage has no effect on the experimental conclusion and accuracy.

Figure 3a shows the mass loss of FeS_2 in different mixed gases. It can be found that the mass loss of samples in each atmosphere exceeds 27%. In fact, the mass loss ratio of the reaction for which FeS_2 is fully converted to FeS is about 26.67%. More than 26.67% of the mass loss is caused by other compound reactions and water vaporization. Besides, the final mass loss of the sample decreases with the increase of H_2 ratio. This is because the increase of H_2 concentration improves the reducibility of the mixed gas. There may be a trace of solid product FeS that is further reduced to Fe, which leads to the carburization reaction to occur more easily, and thus, the final mass loss of the sample is reduced. Previous work pointed out

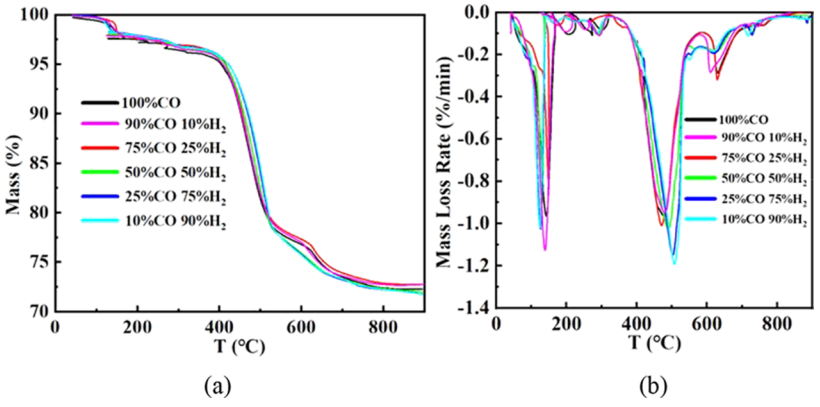

Figure 3. TG (a) and DTG (b) curves of the FeS_2 pyrolysis process under different gas compositions.

https://doi.org/10.1021/acsomega.2c02991
ACS Omega 2022, 7, 29116−29124

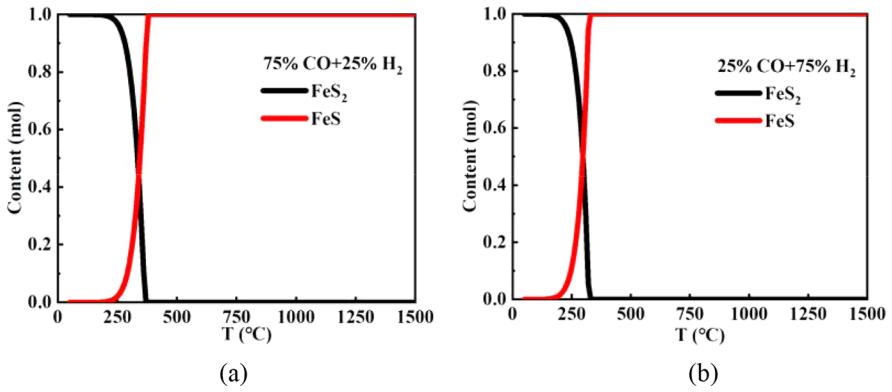

Figure 5. Theoretical calculation of the evolution of FeS_2 in samples under different gas compositions from 0 to 1500 °C: (a) 75% CO + 25% H_2 and (b) 75% CO + 25% H_2.

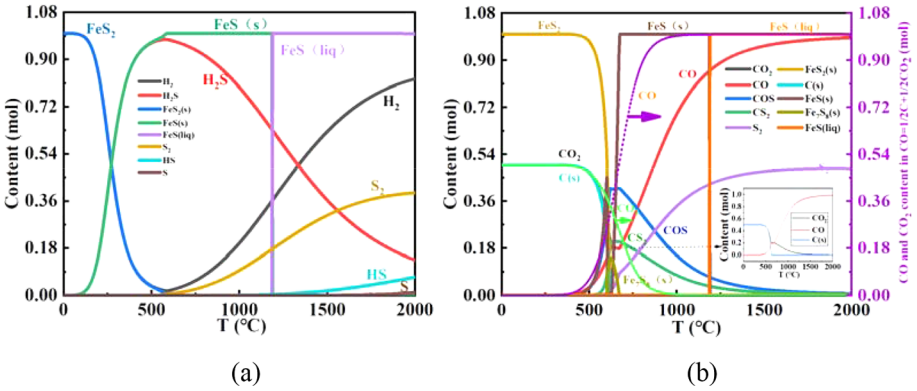

Figure 6. Theoretical calculated variation of product content during FeS_2 reacting with H_2 (a) and CO (b).

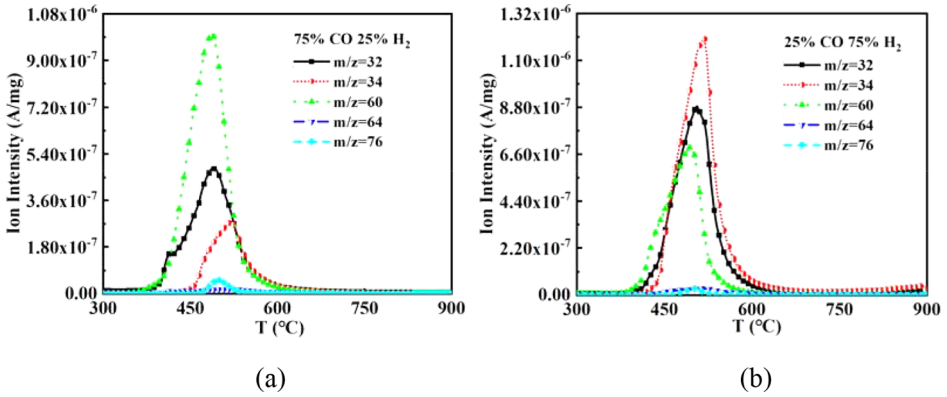

Figure 7. Evolution of gaseous sulfides during the reaction of FeS_2 under different reducing gas compositions: (a) 75% CO + 25% H_2 and (b) 25% CO + 75% H_2.

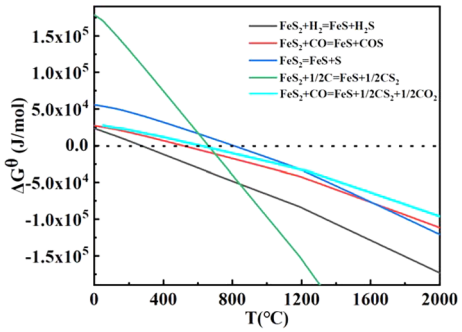

Figure 8. $\Delta G-T$ diagram of FeS_2 reaction.

that the carburization reaction occurs at around 650 °C.[27] As shown in Figure 3a, the carburization clearly occurs around 600 °C (the TG curve with a higher CO concentration clearly has a raised peak at 600 °C). According to Hayashi,[28] traces of sulfur in gas mixtures significantly reduce the carburization rate as the sulfur content increases.

Figure 3b shows the DTG curves under different gas compositions. To eliminate the jaggedness of the curves, the Savitzky−Golay method was employed to smooth curves. The window points and the polynomial order were 150 and 2, respectively. In addition, T_0, $T_{max,}$ and R_m in different atmospheres were extracted to analyze the characteristic temperature, as shown in Table 2. Obviously, T_0 remains

https://doi.org/10.1021/acsomega.2c02991
ACS Omega 2022, 7, 29116−29124

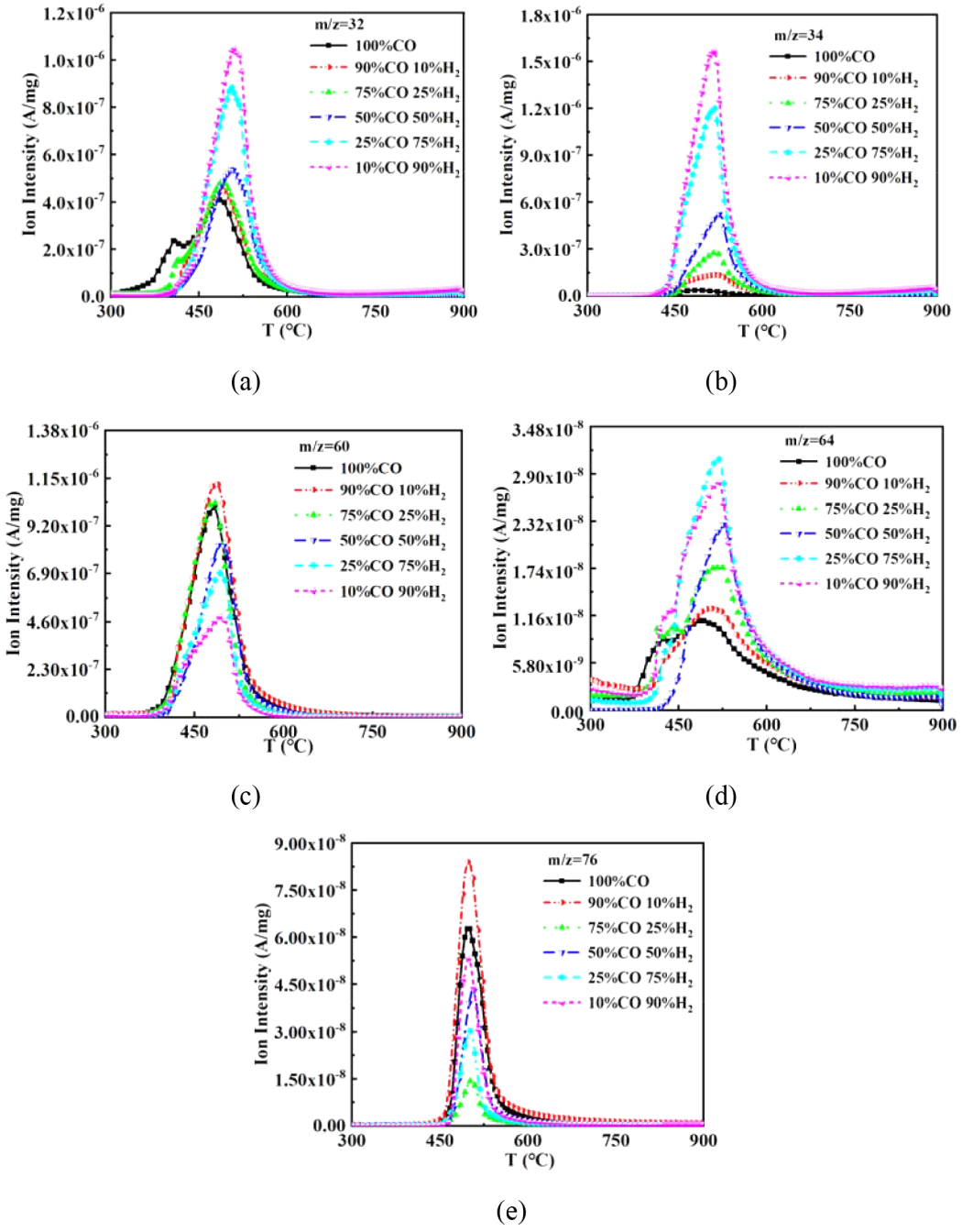

Figure 9. Evolution curves of gaseous sulfides in different mixed gas compositions: (a) m/z = 32, (b) m/z = 34, (c) m/z = 60, (d) m/z = 64, and (e) m/z = 76.

essentially constant for each atmosphere. With the increase of H_2 ratio in the H_2−CO mixtures, R_{max} and T_{max} also increase accordingly. Particularly, the absolute value of R_m slightly increases with the increase of H_2 concentration, indicating that the reduction of the mixed gas increases. The presence of CO limits the maximum decomposition temperature of FeS_2 because at lower H_2 concentrations, the maximum decomposition rate peaks at T_{max}. If the maximum decomposition rate is to be further increased, the gas reduction and temperature need to be increased, resulting in an increase in T_{max} and R_{max} with the increase of H_2 ratio. At the same time, due to the small molecular size of H_2, it is easier to diffuse into the FeS_2 core for reaction, thus promoting its decomposition rate.

3.2. Mineralogy of the Solid Products. Figure 4 shows the XRD patterns for the solid products after pyrolysis. All the samples are with similar mineralogy. FeS is found in the solid product, indicating that the FeS_2 in the sample is almost completely reacted to form FeS. In addition, there are SiO_2 and CaS present in the solid phase before and after the reaction, indicating that these trace impurities in the raw materials do not participate in the reaction. Although the difference in the composition of the mixed gas leads to slightly different reaction rates and characteristic temperatures, there was no effect on the solid product.

Figure 5 shows the evolution of FeS_2 in the samples by thermodynamic calculation. During the pyrolysis of FeS_2 in the CO−H_2 atmosphere, FeS_2 is directly converted to FeS, which

https://doi.org/10.1021/acsomega.2c02991
ACS Omega 2022, 7, 29116−29124

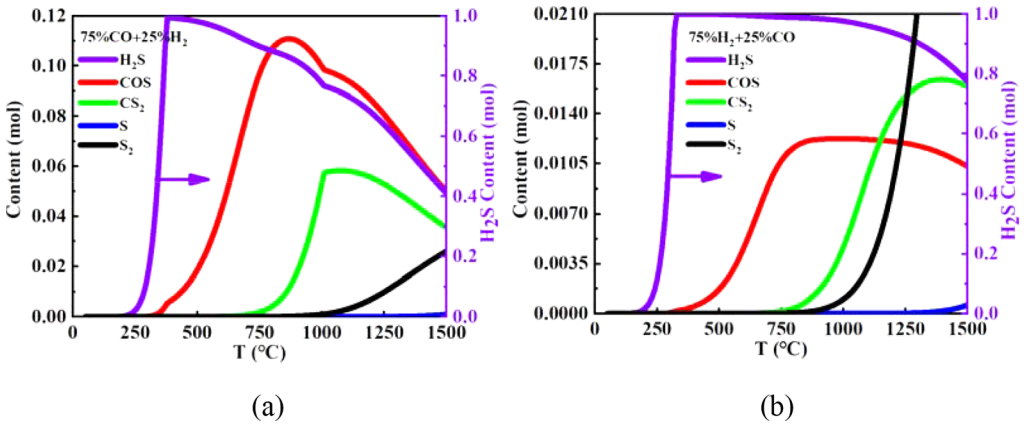

Figure 10. Theoretical calculation of the release of gaseous sulfides in FeS_2 under different ratios of CO and H_2: (a) 75% CO + 25% H_2 and (b) 25% CO + 75% H_2.

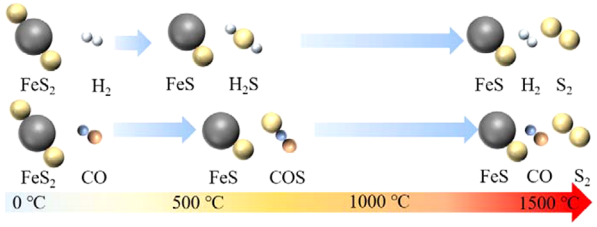

Figure 11. Decomposition process of FeS_2 in the H_2 and CO atmosphere.

is consistent with the experimental data. According to previous studies on the mechanism of FeS_2 decomposition,[16,19,20,29] it is known that FeS_2 decomposition first produces intermediate products such as Fe_7S_8 and then decomposes to produce FeS. Moreover, the increase of H_2 concentration reduces the decomposition temperature of FeS_2, indicating that the increase of H_2 concentration improves the reducibility of the gas and promotes the decomposition of FeS_2.

Note that the initial decomposition temperature of FeS_2 in the calculations (200 °C) is different from that in experiments (350 °C, as shown in Figure 3). This is because the calculations only considered the thermodynamic conditions of the reaction and ignored the kinetic factors. However, chemical reactions are affected by both thermodynamic and kinetic conditions. Considering factors such as gas diffusion, the reaction rate at 200 °C was extremely slow that no reaction was observed in the experiment. The progress of the reaction can only be detected when the temperature is further increased. Although there are differences between thermodynamic calculations and experimental results, the calculated results can help us understand the thermodynamic conditions and the products of the reaction.

Figure 6 indicates that at low temperature, CO is converted into CO_2 due to the carbon deposition reaction ($2CO = C + CO_2$), and FeS_2 reacts with CO_2 to form Fe_7S_8 (found in the reaction products). The produced Fe_7S_8 continues to react with CO and is completely reduced to FeS at the temperature of 675 °C. Therefore, an inflection point of CO concentration appears around this temperature. Before that, the CO content is mainly related to the amount of reduction to FeS and the gas balance, and if the temperature continued to increase, it was only related to the gas balance.

According to Figure 6a, H_2 and FeS_2 start to react at about 100 °C to form H_2S, and the reaction lasts until 580 °C (eq 1). A slight difference between the trend of H_2S and FeS can be seen at about 500 °C, which indicates that H_2S starts to decompose into H_2 and S_2 at 500 °C (eq 2). The content of H_2S decreases significantly after 580 °C. FeS_2 is completely converted into FeS. This indicates that only the decomposition of H_2S occurs after this temperature. At 1190 °C, FeS melts into the liquid state. In addition, a small amount of H_2 and S_2 reacted after 1070 °C to produce HS (eq 3)[30−32]

$$FeS_2 + H_2 = FeS + H_2S \quad (1)$$

$$2H_2S = 2H_2 + S_2 \quad (2)$$

$$H_2 + S_2 = HS \quad (3)$$

As shown in Figure 6b, it can be seen that the content of CO decreases in all reactions with FeS_2 compared to the single reaction $2CO = CO_2 + C$ at 400 °C, which indicates that CO reacts with FeS_2 (eq 4). Besides, the subsequent decrease in CO_2 content is mainly caused by the gas balance after CO is reacted. After 670 °C, COS starts to decompose (eq 5). After 600 °C, the carbon content decreases sharply and the CO_2 content decreases slowly, indicating that carbon is involved in the reaction. At this time, the CS_2 content increases, but the S_2 content has not yet increased, indicating that carbon reacts with FeS_2 to produce CS_2 (eq 6). After 670 °C, the contents of CS_2 and CO_2 show a similar downward trend, while the contents of CO and S_2 increase, indicating that CS_2 reacted with CO_2 to form S_2 and CO (eq 7)[33−36]

$$CO + FeS_2 = COS + FeS \quad (4)$$

$$2COS = 2CO + S_2 \quad (5)$$

$$C + 2FeS_2 = CS_2 + 2FeS \quad (6)$$

$$CO_2 + CS_2 = 2CO + S_2 \quad (7)$$

3.3. Generation of Gaseous Sulfides. Figure 7 shows the mass spectrometry (MS) results during the pyrolysis of pyrite; the inorganic compounds with m/z = 32, 34, 60, 64, and 76 were detected during the experiments. According to previous analysis,[37] FeS_2 catalyzes the reaction of H_2 and CO to produce methanol (m/z = 34) only at low temperatures, while the temperature in this experiment is higher than 400 °C, lacking the generating conditions of methanol, and m/z = 34 therefore represents H_2S. As the gases in the experiment are H_2 and CO, oxygen cannot exist stably in such a strong reducing atmosphere, so m/z = 32 represents sulfur monomers. As

https://doi.org/10.1021/acsomega.2c02991
ACS Omega 2022, 7, 29116−29124

discussed in Figure 6, the sulfur monomers generated from FeS_2 will immediately react with H_2 or CO under current experimental conditions, so the signal of sulfur in the mass spectrum is the m/z = 32 signal produced by the experimental gas molecules after electron bombardment. m/z = 60 is COS, and m/z = 76 is carbon disulfide. Since FeS_2 is decomposed to produce sulfur vapor during the experiment and thermodynamic calculation results show the existence of S_2 (Figure 6b), m/z = 64 in the mixed gas represents S_2.

It can be observed that although the volume fraction of H_2 in the mixed gas is different, the temperature at which all inorganic sulfides begin to generate is around 400 °C, and the peak generation temperature is about 480−550 °C. The peak temperature of gaseous sulfide generation and the end temperature of the reaction both decrease with the increase of the volume fraction of H_2. It means that H_2 reduces the decomposition temperature of FeS_2. Moreover, with the increase of the proportion of H_2, the amount of H_2S (m/z = 34) in the evolved gaseous sulfide gradually increases and exceeds that of COS (m/z = 60). It means that H_2 contributes to the conversion of the gaseous products of FeS_2 decomposition from COS to H_2S. At the same time, CO contributes to the conversion of the gaseous product of FeS_2 decomposition from H_2S to COS. In the current CO−H_2 mixed atmosphere, with the increase of temperature, gaseous sulfides begin to be produced in the following order: COS → S → H_2S → S_2 → CS_2.

The standard free energies with temperature ($\Delta G-T$ diagram) for various possible reactions with FeS_2 are shown in Figure 8. Based on thermodynamic equilibrium calculation results, as the temperature increases, the order of sulfide generation should be H_2S → COS → CS_2 → S (or S_2). It can be found that the generation order of sulfides obtained by the calculation is slightly different from the experimental results. This is because the calculation involves an ideal equilibrium state of a single atmosphere, ignoring the actual kinetic conditions, while the experiment involves a mixed atmosphere. Different from the earliest appearance of H_2S in the theoretical calculation, COS is the earliest generated in the experiments.

According to Aylmore and Lincoln,[29] it is possible that COS is generated by the reaction shown in eq 8. The sulfur in this experiment mainly comes from the decomposition of H_2S and the disproportionation cleavage of FeS_2. According to the calculation results in Figures 6 and 8, none of these reactions can be satisfied under conditions below 400 °C. Figure 7 shows that COS is generated prior to H_2S, which may be due to the immediate reaction of H_2S that is generated before COS with CO to form COS (eq 9). The mass spectral signal of H_2S is generated only after gas equilibrium is reached, and thus, the COS content in the experiment increases before H_2S[34,38]

$$CO + S = COS \quad (8)$$

$$CO + H_2S = COS + H_2 \quad (9)$$

Compared with the calculation results, the lower sulfur generation temperature in the experiment is due to the electron bombardment of COS molecules to generate the m/z = 32 signal. In general, the calculation results are consistent with the experimental results, and the calculation results can reasonably explain the experimental phenomena.

Figure 9 shows the evolution curves of gaseous sulfide in various gas mixtures. m/z = 32, 34, 60, 64, and 76 represent S, H_2S, COS, S_2, and CS_2, respectively. As shown in Figure 9a, the content of generated sulfur of FeS_2 increases gradually with the increase of H_2 concentration, and the T_{max} of generated sulfur is around 480 °C, which indicates that H_2 promotes the generation of sulfur from FeS_2. Figure 9b shows that with the increase of H_2 concentration, the overall content of H_2S is gradually increased, while the T_0 decreases. It means that H_2S is mainly produced by reaction of eq 1, and H_2 decreases the generation temperature of sulfur in FeS_2. As shown in Figure 9c, it also shows that the COS content increases overall with increasing CO concentration, but the COS content at 100% CO is slightly lower than that at 75% CO and 90% CO. According to Figure 6, H_2 is able to react with FeS_2 at around 100 °C, so the sulfur in FeS_2 can be preferentially carried out by H_2, which in turn reacts with CO and CO_2 to form COS. In 100% CO atmosphere, only CO can react with FeS_2 and the reaction temperature is around 400 °C. Therefore, the lower COS content in 100% CO atmosphere compared to 90 and 75% CO atmosphere is the part of sulfur carried out by H_2 in the early stage. For Figure 9d, it can be found that the generation of S_2 molecules gradually increases with the increase of H_2 concentration, which further indicates that H_2 promotes the generation of sulfur in FeS_2. In Figure 9e, the production of CS_2 reaches the peak at around 500 °C, but there is no significant regularity in the production of CS_2 under different H_2 concentrations. We speculate that this is due to the extremely low production of CS_2 and the error of the device detection.

In general, the increase of H_2 concentration favors the generation of S, H_2S, and S_2 and reduces the temperature of sulfide decomposed from FeS_2. However, the increase of CO concentration is beneficial for the generation of COS and CS_2, and the temperature range of sulfide generation is 400−600 °C.

Figure 10 shows the release of gaseous sulfides in FeS_2 under different ratios of CO and H_2 by calculations. Obviously, with the increase of reaction temperature, the sequence of gaseous sulfide release is H_2S → COS → CS_2 → S_2 → S, which is consistent with the order in the $\Delta G-T$ diagram, as shown in Figure 8. The calculation principle is based on the minimum Gibbs free energy of the chemical reaction, and the final result is the equilibrium state. At around 350 °C, the H_2S content peaks, along with a small amount of COS. According to Figure 8, CO is not yet able to react directly with FeS_2 at this temperature, indicating that COS is formed by the reaction of H_2S and CO (eq 9), which further verifies the previous view. In the gas mixture, H_2S starts to be released at about 200 °C, and its content reaches a peak at about 350 °C and then decreases slowly. Simultaneously, the contents of COS and CS_2 start to increase significantly after 350 °C, indicating that the generation temperature of COS and CS_2 is higher than that of H_2S. Moreover, the concentrations of COS and CS_2 released are obviously higher in 75% CO + 25% H_2 mixture, while those of H_2S and S_2 are obviously higher in 25% CO + 75% H_2 mixture. It means that CO promotes the release of COS and CS_2, and H_2 promotes the release of H_2S and S_2. This is consistent with the conclusions obtained from the experimental results.

After the above discussions, the pyrolysis behavior of FeS_2 in the CO and H_2 mixed atmosphere has been clarified, and the schematic diagram of the reaction mechanism is shown in Figure 11. FeS_2 reacts with H_2 to produce H_2S. At the high-temperature stage, the generated H_2S decomposes to produce H_2 and S_2. In a CO atmosphere, FeS_2 reacts with CO to

https://doi.org/10.1021/acsomega.2c02991
ACS Omega 2022, 7, 29116−29124

produce COS and a small amount of CS_2. At the high-temperature stage, COS and CS_2 decompose to produce CO and S_2.

4. CONCLUSIONS

In this work, the experiments and thermodynamic calculations were combined to investigate the pyrolysis process of FeS_2 under the mixed atmosphere of CO and H_2. The effects of temperature and H_2 ratio on the pyrolysis products including solid and gaseous products were analyzed. Under the current experimental conditions, the following conclusions can be drawn.

- The final solid products from the decomposition of FeS_2 in different proportions of CO and H_2 mixed gases are all FeS. The difference is that FeS_2 is directly reduced to FeS by reaction with H_2, while it will be reduced to Fe_7S_8 and then reduced to FeS when it reacts with CO.
- H_2S and COS are main gaseous sulfides formed by the decomposition of FeS_2 in the CO−H_2 atmosphere. The temperature at which gaseous sulfides start to release is about 300 °C. All H_2S are directly generated by the reaction of FeS_2 with H_2. Some COS is directly generated by the reaction of FeS_2 with CO. The other is formed by the reaction of CO with H_2S or S_2.
- higher H_2 concentration can reduce the pyrolysis reaction temperature of FeS_2, which is favorable for the conversion of sulfides to H_2S, while a higher CO concentration promotes the conversion of sulfides to COS.
- When FeS_2 reacts with H_2 and CO mixed gas, the order in which gaseous sulfides are produced with increasing temperature is as follows: COS → S → H_2S → S_2 → CS_2. The decomposition temperature is generally from 400 to 800 °C, and a temperature higher than 800 °C will be more favorable for the release of COS and CS_2.

AUTHOR INFORMATION

Corresponding Authors

Yang You − *College of Materials Science and Engineering, Chongqing University, Chongqing 400044, China;* orcid.org/0000-0002-5403-0673; Email: youyang@cqu.edu.cn

Xuewei Lv − *College of Materials Science and Engineering, Chongqing University, Chongqing 400044, China;* Email: lvxuewei@cqu.edu.cn

Authors

Zhuang Zheng − *College of Materials Science and Engineering, Chongqing University, Chongqing 400044, China*

Jiabao Guo − *College of Materials Science and Engineering, Chongqing University, Chongqing 400044, China*

Gang Li − *College of Materials Science and Engineering, Chongqing University, Chongqing 400044, China*

Zhixiong You − *College of Materials Science and Engineering, Chongqing University, Chongqing 400044, China*

Complete contact information is available at: https://pubs.acs.org/10.1021/acsomega.2c02991

Notes

The authors declare no competing financial interest.

ACKNOWLEDGMENTS

This work was supported by the National Natural Science Foundation of China (52004046, 51974048), the China Postdoctoral Science Foundation (2021T140783, 2020M673131), and the Postdoctoral Science Foundation of Chongqing (cstc2020jcyj-bshX0030).

REFERENCES

(1) Pyshyev, S.; Shevchuk, K.; Chmielarz, L.; Kuśtrowski, P.; Pattek-Janczyk, A. Effect of the water-vapor content on the oxidative desulfurization of sulfur-rich coal. *Energy Fuels* **2007**, *21*, 216−221.

(2) Frilund, C.; Kotilainen, M.; Barros Lorenzo, J.; Lintunen, P.; Kaunisto, K. Steel Manufacturing EAF Dust as a Potential Adsorbent for Hydrogen Sulfide Removal. *Energy Fuels* **2022**, *36*, 3695−3703.

(3) Meng, X.; Yang, J.; Ye, Z.; Chu, R.; Wang, C.; Li, W.; et al. Effect of ash − ZnO heat carrier on sulfur migration behavior during pyrolysis of coal. *Fuel* **2022**, *308*, 121993.

(4) Carpenter, A. CO_2 abatement in the iron and steel Industry. *IEA Clean Coal Centre* **2012**, *25*, 193.

(5) Lanzerstorfer, C.; Preitschopf, W.; Neuhold, R.; Feilmayr, C. Emissions and Removal of Gaseous Pollutants from the Top-gas of a Blast Furnace. *ISIJ Int.* **2019**, *59*, 590−595.

(6) Lu, Z.; Gu, H.; Chen, L.; Liu, D.; Yang, Y.; McLean, A. A review of blast furnace iron-making at Baosteel facilities. *Ironmaking Steelmaking* **2019**, *46*, 618−624.

(7) Wei, Z.; Zhang, X.; Zhang, F.; Xie, Q.; Zhao, S.; Hao, Z. Boosting carbonyl sulfide catalytic hydrolysis performance over N-doped Mg-Al oxide derived from MgAl-layered double hydroxide. *J. Hazard. Mater.* **2021**, *407*, 124546.

(8) Nimthuphariyha, K.; Usmani, A.; Grisdanurak, N.; Kanchanatip, E.; Yan, M.; Suthirakun, S.; et al. Hydrolysis of carbonyl sulfide over modified Al2O3 by platinum and barium in a packed-bed reactor. *Chem. Eng. Commun.* **2021**, *208*, 539−548.

(9) Jiang, G.; Zhang, X.; Zhang, F.; Liu, Z.; Wang, Z.; Hao, Z.; et al. Efficient recovery of hydrogen and sulfur resources over non-sulfide based LaFexAl12-xO19 hexaaluminate catalysts by H2S catalytic decomposition. *Appl. Catal., B* **2020**, *263*, 118354.

(10) Shimomura, Y.; Nishikawa, K.; Arino, S.; Katayama, T.; Hida, Y.; Isoyama, T. On the inside state of the lumpy zone of blast furnace. *Tetsu-to-Hagane* **1976**, *62*, 547.

(11) Wada, K.; Ishimitsu, A. Study on behaviour of the sulphur in the blast furnace. *Tetsu-to-Hagane* **1952**, *38*, 623−630.

(12) Edreis, E. M. A.; Li, X.; Luo, G.; Sharshir, S. W.; Yao, H. Kinetic analyses and synergistic effects of CO2 co-gasification of low sulphur petroleum coke and biomass wastes. *Bioresour. Technol.* **2018**, *267*, 54−62.

(13) Gornostayev, S.; Härkki, J.; Kerkkonen, O. Transformations of pyrite during formation of metallurgical coke. *Fuel* **2009**, *88*, 2032−2036.

(14) Li, X.; Wang, X.; Wang, L.; Ning, P.; Ma, Y.; Zhong, L.; et al. Efficient removal of carbonyl sulfur and hydrogen sulfide from blast furnace gas by one-step catalytic process with modified activated carbon. *Appl. Surf. Sci.* **2022**, *579*, 152189.

(15) Zhao, H.; Bai, Z.; Yan, J.; Bai, J.; Li, W. Transformations of pyrite in different associations during pyrolysis of coal. *Fuel Process. Technol.* **2015**, *131*, 304−310.

(16) Huang, F.; Zhang, L.; Yi, B.; Xia, Z.; Zheng, C. Transformation pathway of excluded mineral pyrite decomposition in CO_2 atmosphere. *Fuel Process. Technol.* **2015**, *138*, 814−824.

(17) Levy, J.; White, T. The reaction of pyrite with water vapour. *Fuel* **1988**, *67*, 1336−1339.

(18) Thomas, P. S.; Hirschausen, D.; White, R. E.; Guerbois, J. P.; Ray, A. S. Characterization of the oxidation products of pyrite by thermogravimetric and evolved gas analysis. *J. Therm. Anal. Calorim.* **2003**, *72*, 769−776.

(19) Aylmore, M.; Lincoln, F. Mechanochemical milling-induced reactions between gases and sulfide minerals: II. Reactions of CO2

https://doi.org/10.1021/acsomega.2c02991
ACS Omega 2022, 7, 29116−29124

with arsenopyrite, pyrrhotite and pyrite. *J. Alloys Compd.* **2001**, *314*, 103−113.
(20) Lv, W.; Yu, D.; Wu, J.; Zhang, L.; Xu, M. The chemical role of CO2 in pyrite thermal decomposition. *Proc. Combust. Inst.* **2015**, *35*, 3637−3644.
(21) Hong, Y.; Fegley, B., Jr. The kinetics and mechanism of pyrite thermal decomposition. *Ber. Bunsenges. Phys. Chem.* **1997**, *101*, 1870−1881.
(22) Li, G.; Lv, X.; Ding, C.; Zhou, X.; Zhong, D.; Qiu, G. Non-isothermal carbothermic reduction kinetics of calcium ferrite and hematite as oxygen carriers for chemical looping gasification applications. *Appl. Energy* **2020**, *262*, 114604.
(23) Zhang, H.; Xian, S.; Zhu, Z.; Guo, X. Release behaviors of sulfur-containing pollutants during combustion and gasification of coals by TG-MS. *J. Therm. Anal. Calorim.* **2021**, *143*, 377−386.
(24) Yao, H.; Ni, L.; Wu, P.; Jiang, J.; Ni, Y.; Yao, X. Thermal hazard and pyrolysis mechanism of tetrazolo[1,5-a]pyridine by TG, DSC, ARC, TG-MS and DFT methods. *J. Anal. Appl. Pyrolysis* **2021**, *159*, 105299.
(25) Kundu, N.; Biswas, P.; Bhunia, P.; Ghosh, R.; Sarkar, S. Evolution characteristics of metallurgical coals for coke making through thermogravimetric-mass spectroscopic measurements. *J. Environ. Eng.* **2021**, *9*, 106874.
(26) Sahu, S. G.; Sarkar, P.; Chakraborty, N.; Adak, A. K. Thermogravimetric assessment of combustion characteristics of blends of a coal with different biomass chars. *Fuel Process. Technol.* **2010**, *91*, 369−378.
(27) Cai, Y.; Nguyen, T. D.; Zhang, J.; Gleeson, B.; Young, D. Corrosion behaviour of Fe-25Cr alloy in wet CO_2 gas at 650 degrees C: Effects of chloride deposits and Si plus Mn alloying addition. *Corros. Sci.* **2022**, *195*, 110001.
(28) Hayashi, S. Influence of traces of gaseous sulphur on carburisation rate of iron in CO−H_2 mixtures. *Ironmaking Steelmaking* **2014**, *42*, 233−240.
(29) Aylmore, M.; Lincoln, F. Mechanochemical milling-induced reactions between gases and sulfide minerals: I. Reactions of SO2 with arsenopyrite, pyrrhotite and pyrite. *J. Alloys Compd.* **2000**, *309*, 61−74.
(30) Startsev, A. Low-temperature catalytic decomposition of hydrogen sulfide into hydrogen and diatomic gaseous sulfur. *Kinet. Catal.* **2016**, *57*, 511−522.
(31) Wei, X. Y.; Ogata, E.; Zong, Z. M.; Niki, E. Effects of hydrogen pressure, sulfur, and iron sulfide (FeS2) on diphenylmethane hydrocracking. *Energy Fuels* **1992**, *6*, 868−869.
(32) Zhou, C.; Sendt, K.; Haynes, B. S. Theoretical study of reactions in the multiple well H2/S2 system. *J. Phys. Chem. A* **2009**, *113*, 8299−8306.
(33) Harnisch, J.; Borchers, R.; Fabian, P. COS, CS2 and SO2 in aluminium smelter exhaust. *Environ. Sci. Pollut. Res.* **1995**, *2*, 229.
(34) Duan, L.; Zhao, C.; Zhou, W.; Qu, C.; Chen, X. Investigation on Coal Pyrolysis in CO2Atmosphere. *Energy Fuels* **2009**, *23*, 3826−3830.
(35) Calkins, W. H. Investigation of organic sulfur-containing structures in coal by flash pyrolysis experiments. *Energy Fuels* **1987**, *1*, 59−64.
(36) Schoonen, M. A. A.; Xu, Y.; Bebie, J. Energetics and Kinetics of the Prebiotic Synthesis of Simple Organic Acids and Amino Acids with the FES-H2S/FES2 Redox Couple as Reductant. *Origins Life Evol. Biospheres* **1999**, *29*, 5−32.
(37) Zhang, D.; Zhang, J.; Sun, D. Synthesis of cis-1,3,3,3-tetrafluoropropene by catalytic isomerization of trans-1,3,3,3-tetrafluoropropene over alumina catalysts. *Appl. Catal., A* **2020**, *606*, 117800.
(38) Barrault, J.; Boulinguiez, M.; Forquy, C.; Maurel, R. Synthesis of methyl mercaptan from carbon oxides and H_2S with tungsten—alumina catalysts. *Appl. Catal.* **1987**, *33*, 309−330.

https://doi.org/10.1021/acsomega.2c02991
ACS Omega 2022, 7, 29116−29124